J Therm Anal Calorim (2014) 115:987–1001
DOI 10.1007/s10973-013-3466-8

Thermal decomposition and biological activity studies of some transition metal complexes derived from mixed ligands sparfloxacin and glycine

M. H. Soliman · A. M. M. Hindy · G. G. Mohamed

Received: 16 July 2013 / Accepted: 4 October 2013 / Published online: 5 November 2013

Abstract The synthetic method of novel ternary M(II)/(III)/(IV) complexes, with fluoroquinolone drug sparfloxacin (HSFX) and glycine (HGly) containing nitrogen and oxygen donor ligand have been synthesized and characterized. The prepared complexes fall into stoichiometric formulae of $[M(SFX)(Gly)(H_2O)_2]Cl$ (M = Cr(III) and Fe(III), $[M(SFX)(Gly)(H_2O)_2]$ (M = Mn(II), Co(II), Ni(II), Cu(II), Zn(II) and UO_2(II) and $[Th(SFX)(Gly)(H_2O)_2]Cl_2$. The chelate rings are six-membered and six coordinate with 1:1:1 [M]:[SFX]:[Gly]. The important bands in the IR Spectra and main ^{1}H NMR signals are tentatively assigned and discussed in relation to the predicted molecular structure. The IR data of the HSFX and HGly ligands suggested the existing of a bidentate binding involving carboxylate O and carbonyl O for HSFX ligand and amino N and carboxylate O atoms for HGly ligand. The coordination geometries and electronic structures are determined from the diffused reflectance spectra and magnetic moment measurements. The complexes exist in octahedral form. The complexes decomposed in four to six steps within the temperature range 30–1,000 °C with metal oxides as residues of decomposition. The decomposition steps are accompanied by endothermic or exothermic peaks in the DTA. The HSFX drug, HGly and metal complexes have been screened for their in vitro antibacterial activities against *Staphylococcus aureus* and *Escherichia coli*, and antifungal activities against *Aspergillus niger* and *Candida albicans* by MIC method. The metal complexes were found to have higher antimicrobial activity than the HSFX drug and HGly ligand and their activity are comparable with the antibacterial and antifungal standards.

Keywords Sparfloxacin · Glycine · Metal complexes · Thermal analyses · IR · Biological activity

M. H. Soliman (✉)
Chemistry Department, Faculty of Science, Helwan University, P.O. Box 11795, Helwan, Egypt
e-mail: drmadihahasn@yahoo.com

A. M. M. Hindy · G. G. Mohamed
Chemistry Department, Faculty of Science, Cairo University, Giza 12613, Egypt

Introduction

The development of metal complexes as artificial nucleases is an area of interest. Fluoroquinolones derivatives posses a broad spectrum of activity against various pathogenic microorganisms, which are resistant to aminoglycosides, penicilins, cephalosporins, tetracyclines and other antibiotics. This class of compounds, when compared to existing bactericidal drugs, shows improved pharmacokinetic properties and a broad spectrum of activity against parasites, bacteria and mycobacteria, including resistant strains; in addition to that they displayed significant in vitro antibacterial activity against many Gram-positive and Gram-negative bacteria through inhibition of their DNA gyrase [1]. Sparfloxacin (HSFX, 5-amino-1-cyclopropyl-7-(*cis*-3,5-dimethypiperazino)-6,8-difluoro-1,4-dihydro-4-oxo-3-quinoline carboxylic acid) Fig. 1 is widely used in the treatment of urinary tract infections and is reported to exhibit higher activity against the major respiratory pathogens and typical pathogens that cause pneumonia [2].

Metal coordination to biologically active molecules can be used in order to enhance their biological activity; therefore, numerous studies regarding the interaction between quinolones with several metallic cations have reported in the literature [3, 4]. Some of these metal

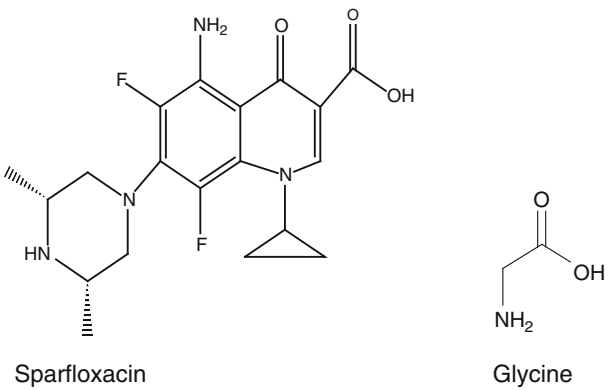

Fig. 1 Structure of sparfloxacin and glycine ligands

complexes presented potential antibacterial activity [5, 6], for example Co(II) and Cu(II) complexes with sparfloxacin exhibited a significant enhancement against several pathogenic bacteria than sparfloxacin [7]. The antibacterial and antifungal properties of palladium and platinum complexes with sparfloxacin have also been reported, where the complexes showed activity against *Mycobacterium tuberculosis* strain [8]. Ciprofloxacin behaved as bidentate ligand binding to the metallic ion through the carboxylate and carbonyl oxygens as observed in case of Co(II), Ni(II), Zn(II), Cd(II), Mn(II) and Cu(II) complexes [9]. Nevertheless, it was mentioned that platinum complexes were chelated with fluoroquinolones via piperazine nitrogen atoms which is much less common [8]. Recently, some transition and earth metal complexes of sparfloxacin were prepared and characterized and antifungal activity was evaluated where Fe(II) and Cd(II) complexes showed remarkable activity [10]. All the binary and ternary complexes showed remarkable potential antimicrobial activity higher than the recommended standard agents [11, 12].

Thermal analysis techniques, in which a physical property is monitored as a function of temperature or time while the analyte is heated or cooled under controlled conditions, are fundamental techniques for the characterization of drugs and drug products, not only while processing or ageing conditions may be simulated but while the methods gives access to thermodynamic data. Due to the different informations delivered, thermal analysis methods are concurrent or complementary to other analytical techniques, such as spectroscopy, chromatography, melting, loss on drying, assay, for identification, purity and quantitation. They are basic methods in the field of polymer analysis and in physical and chemical characterization of pure substances as well as for mixtures. They find good applications for preformulation, processing and control of the drug product. The introduction of automation considerably increases the advantages of these methods. Thermogravimetry (TG) and differential scanning calorimetry (DSC) are useful techniques that have been successfully applied in the pharmaceutical industry to reveal important information regarding the physicochemical properties of drug and excipient molecules such as polymorphism, stability, purity, formulation compatibility among others. Thermal behaviour of binary and ternary metal complexes of some fluoroquinolones have been reported [8, 10–15]. The thermal decomposition of the complexes is discussed and the thermodynamic data are reported using Coats-Redfern and/or Horowitz–Metzeger equations [11, 14–17]. Therefore, in this article, synthesis, spectroscopic and thermal characterization of ternary Cr(III), Mn(II), Fe(III), Co(II), Ni(II), Cu(II), Zn(II), UO_2(II) and Th(IV) complexes of sparfloxacin in presence of glycine are reported using physicochemical techniques such as elemental analysis, molar conductance, magnetic susceptibility, IR, UV–Vis, thermal analysis and ^{1}H-NMR spectral studies. The antimicrobial activity of HSFX, HGly and the ternary complexes has been screened against Gram-positive and Gram-negative bacteria. Antifungal activity against two different fungi has been evaluated and compared with reference drug. All the ternary complexes showed remarkable potential antimicrobial activity higher than the recommended standard agents.

Experimental

Materials and reagents

All chemical used were of the analytical reagent grade (AR) and of highest purity available. They included sparfloxacin (Unifram, Egypt) and glycine (The drug houses B.D.H laboratory chemicals division poole England). $CuCl_2{\cdot}2H_2O$, $NiCl_2{\cdot}6H_2O$, $CrCl_3{\cdot}6H_2O$, $UO_2(NO_3)_2$ and $CoCl_2{\cdot}6H_2O$ were supplied from Sigma. $ZnCl_2{\cdot}2H_2O$ (Ubichem), $FeCl_3{\cdot}6H_2O$ (Prolabo) and $ThCl_4$ (Aldrich) were also used. Hydrogen peroxide, sodium carbonate, sodium hydroxide, hydrochloric, nitric, phosphoric, acetic and boric acids were supplied from Merck. The organic solvents (ethanol, diethylether and dimethylformamide (DMF) were spectroscopic pure from BDH. Bi-distilled water was used in all preparations [19].

Solutions

Fresh stock solutions of 1×10^{-3} mol dm^{-3} HSFX and glycine ligands were prepared by dissolving the accurately weighed amounts of HSFX (0.39241 g dm^{-3}) and glycine (0.075 g dm^{-3}) in the appropriate volume of absolute ethanol. 1×10^{-3} mol dm^{-3} Stock solutions of the metal salts (Fe(III), 0.27 g dm^{-3}; Co(II), 0.23 g dm^{-3}; Ni(II), 0.23 g dm^{-3}; Cu(II), 0.17 g dm^{-3}; Zn(II), 0.172 g dm^{-3};

Table 1 Analytical and physical data of ternary complexes

Complex	Colour/% yield	Found (Calcd.)/%					μeff/B.M.
		C	H	N	Cl	M	
$[Cr(SFX)(Gly)(H_2O)_2]Cl$	Brown	42.66	4.99	11.56	5.48	8.54	3.95
$C_{21}H_{29}Cr\ ClF_2N_5O_7$	(85)	(42.82)	(4.92)	(11.89)	(5.94)	(8.83)	
$[Mn(SFX)(Gly)(H_2O)_2]$	Dark blue	45.51	5.49	12.89	–	9.57	5.55
$C_{21}H_{29}MnF_2N_5O_7$	(72)	(45.29)	(5.21)	(12.58)		(9.88)	
$[Fe(SFX)(Gly)(H_2O)_2]Cl$	White	42.87	4.47	11.49	5.53	9.83	5.36
$C_{21}H_{29}FeClF_2N_5O_7$	(73)	(42.53)	(4.89)	(11.81)	(5.90)	(9.45)	
$[Co(SFX)(Gly)(H_2O)_2]$	Green	44.61	5.49	12.78	–	10.99	5.74
$C_{21}H_{29}CoF_2N_5O_7$	(87)	(44.96)	(5.17)	(12.49)		(10.52)	
$[Ni(SFX)(Gly)(H_2O)_2]$	Pale brown	44.54	5.56	12.89	–	10.23	3.59
$C_{21}H_{29}NiF_2N_5O_7$	(93)	(44.99)	(5.17)	(12.49)		(10.48)	
$[Cu(SFX)(Gly)(H_2O)_2]$	Dark green	44.29	5.41	12.11	–	11.58	1.88
$C_{21}H_{29}CuF_2N_5O_7$	(91)	(44.60)	(5.13)	(12.39)		(11.24)	
$[Zn(SFX)(Gly)(H_2O)_2]$	Dark blue	44.21	5.47	12.48	–	11.87	Diam.
$C_{21}H_{29}ZnF_2N_5O_7$	(86)	(44.46)	(5.11)	(12.35)		(11..53)	
$[Th(SFX)(Gly)(H_2O)_2]Cl_2$	Yellow	31.72	3.22	8.40	8.23	28.42	Diam.
$C_{21}H_{29}Th\ Cl_2F_2N_5O_7$	(79)	(31.36)	(3.60)	(8.71)	(8.71)	(28.87)	
$[UO_2(SFX)(Gly)(H_2O)_2]$	Pale yellow	32.47	3.45	9.41	–	30.49	Diam.
$C_{21}H_{29}UF_2N_5O_9$	(74)	(32.66)	(3.75)	(9.07)		(30.85)	

Cr(III), 0.26 g dm^{-3}; UO_2(II), 0.50 g dm^{-3}, Mn(II), 0.16 g dm^{-3} and Th(IV), 0.37 g dm^{-3}) were prepared by dissolving the accurately weighed amounts of the metal salts in the appropriate volume of bi-distilled water [11].

Instruments

Infrared spectra were recorded on a Perkin-Elmer FT-IR type 1650 spectrophotometer in wave number region 4,000–400 cm^{-1}, where the spectra were recorded as KBr pellets. The pH measurements were carried out using Jenway 3505 pH meter UK. Elemental microanalyses of the separated solid chelates for C; H, N and Cl were performed using CHN-932(LECO) Vario Elemental Analyzer. The analyses were repeated twice to check the accuracy of the data. Spectrophotometric measurements were performed by Shimadzu UV-mini-1240 spectrophotometer. The molar conductance is measured in solution of 10^{-3} mol dm^{-3} of metal complexes in DMF using Jenway 4010 conductivity meter. The solid reflectance spectra were measured on a Shimadzu 3101 pc spectrophotometer. The molar magnetic susceptibility was measured on powdered samples using the Faraday method. The diamagnetic corrections were made by Pascal's constant and $Hg[Co(SCN)_4]$ was used as calibrant. Analyses of the metals followed the dissolution of the solid complex in concentrated HNO_3, neutralizing the diluted aqueous solutions with ammonia and titrating the metal solutions with EDTA. Mass spectra were recorded by the EI technique at 70 eV using MS-5988 GS-MS Hewlett-Packard instrument at the Microanalytical Center, National Center for Research, Egypt. The ^{1}HMNR spectra were recorded using 300 MHz Varian-Oxford Mercury. The deuterated solvent used was dimethylsulphoxide (DMSO-d_6) and the spectra extended from 0 to 15 ppm. The thermal analyses (TG, DTG and DTA) were carried out in dynamic nitrogen atmosphere (20 mL min^{-1}) with a heating rate of 10 °C min^{-1} using Shimadzu TG-50H thermal analyzers. The antibacterial and antifungal activities were evaluated at the Microbiological Laboratory, Microanalytical Center, Cairo University.

Synthesis of metal complexes

The ternary metal complexes were prepared by the addition of hot solution (60 °C) of the appropriate metal chloride or nitrate (1.0 mmol) in an ethanol–water mixture (1:1, 20 mL) to the hot ethanolic solution (60 °C) of the mixture of (0.4 g HSFX, 0.77 g glycine, 1.0 mmol) by molar ratio 1:1:1 [M]:[SFX]:[Gly]. The resulting mixture was stirred under reflux for half hour. The pH of the solution was adjusted with ethanolic ammonia solution whereupon the complexes precipitated, then removed by filtration, washed with hot ethanol followed by diethylether and dried in vaccum desiccator over anhydrous calcium chloride. The analytical data for C, H, N and Cl were repeated twice.

Scheme 1 Mass fragmentation pattern of sparfloxacin

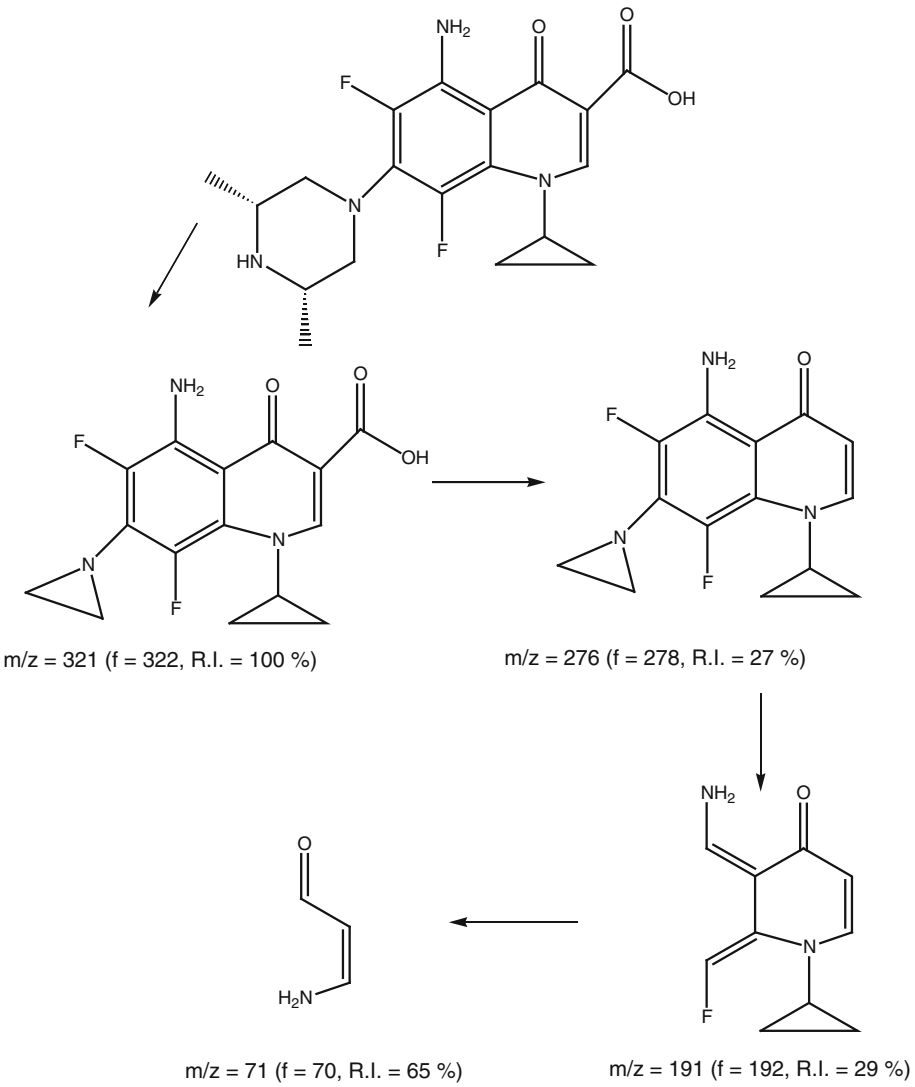

Biological activity

Antimicrobial activity of the tested samples was determined using a modified-Kirby–Bauer disc diffusion method [19]. 100 µL of the tested bacteria or fungi were grown in 10 mL of fresh media until they reached a count of approximately 108 and 105 cells mL^{-1} for bacteria and fungi, respectively [20]. 100 µL of microbial suspension was spread onto agar plates corresponding to the broth in which they were maintained. Isolated colonies of each organism that might be play a pathogenic role were selected from primary agar plates and tested for susceptibilities by disc diffusion method. Of the many media available, NCCLS recommends Mueller–Hinton agar due to: it results in good batch-to-batch reproducibility. Disc diffusion method for filamentous fungi tested by using approved standard method (M38-A). For evaluating the susceptibilities of filamentous fungi to antifungal agent, disc diffusion method for yeast was developed by using approved standard method (M44-P) [21]. Plates inoculated with filamentous fungi as A*sprgillus flavus* at 25 °C for 48 h; Gram (+) bacteria as *Staphylococcus aureus*; Gram (−) bacteria as *Escherichia coli*, they were incubated at 35–37 °C for 24–48 h and yeast as *Aspergillus niger and Candida albicans* incubated at 30 °C for 24–28 h. Then, the diameters of the inhibition zones were measured in millimeters [22]. Standard discs of tetracycline (antibacterial agent), and amphotericin B (antifungal agent) served as positive controls for antimicrobial activity but filter discs impregnated with 10 µL for solvent (distilled water, chloroform, DMSO) were used as a negative control. The agar used is Mueller–Hinton agar that is rigorously tested for composition and pH. Further the depth of the agar in the plate is a factor to be considered in the disc diffusion method. This method is well documented and standard zones of inhibition have been determined for susceptible

Table 2 IR spectral data (4,000-400 cm^{-1}) of HSFX, HGly and ternary metal complexes

Assignment	HSFX	HGly.	Cr(III)	Mn(II)	Fe(III)	Co(II)	Ni(II)	Cu(II)	Zn(II)	Th(IV)	UO_2(II)
NH_{2As} stretch	3,462s	3,400br	3,247sm	3,414br	3,293m	3,412br	3,412br	3,441br	3,413s	3,415br	3,431br
N–H_{as}	3,461s	–	3,444sm	3,412br	3,479br	3,419br	3,420br	3,430sm	3,443br	3,415br	3,464br
N–Hs	3,338s	–	3,334sm	3,323br	3,355br	3,334br	3,334br	3,323sm	3,323br	3,350br	3,358br
CH_{As} stretch	3,092s	3,155br	3,152sm	2,921sm	2,975sm	3,160sm	3,155br	3,116br	3,148br	2,934br	2,929sm
CH stretch in CH_3 and in CH_2 groups	3,092sm	–	3,092br	3,092br	3,090br	3,095br	3,090br	3,092br	3,092br	3,095br	3,092br
CH_s stretch	–	2,896br	2,890br	2,843sm	2,850sm	2,890sm	2,886br	2,894sm	2,973sm	2,879br	2,926sm
C=O stretch	1,716s	1,703sm	1,713m	Dis	1,712sm	1,710sm	1,712 m	Dis	1,699sm	Dis	Dis
COO asym.	–	1,556m	1,575m	1,565br	1,535m	1,593sm	1,560sm	1,550sm	1,563sm	1,570br	1,567sm
COO asym.	1,532m	–	1,516m	1,540w	1,510s	1,540s	1,530sm	1,525sm	1,530sm	1,530m	1,530m
CH_2 deformation	1,438s	–	1,441m	1,447m	1,444m	1,440m	1,456sm	1,444m	1,445m	1,446m	1,441m
COO sym.	–	1,413sm	1,400w	1,390m	1,375m	1,400s	1,399m	1,397sm	1,396sm	1,397sm	1,385m
COO sym.	1,332sm	–	1,340m	1,300s	1,328s	1,310w	1,300m	1,298s	1,297s	1,298s	1,290s
C–N stretch and C–C vibration	1,225m	–	1,250sm	1,230s	1,247m	1,220w	1,250sm	1,250w	1,260m	1,240w	1,270w
Coordinated H_2O	–	–	992m	923sm	914m	920sm	940m	924sm	930sm	940m	923m
			850sm	842m	812s	845m	841m	847m	843m	820m	816sm
C–F stretch	670sm	–	684sm	684m	689m	686sm	692sm	690sm	688m	684m	687m
C–F stretching	638sm	–	631sm	630sm	628sm	632m	630m	628sm	636sm	627sm	634sm
M–O	–	540sm	515sm	518sm	508s	517sm	520sm	531sm	512sm	504sm	527sm
M–O coordinated water	–	–	458sm	452sm	461sm	460sm	458sm	442sm	460sm	453sm	454sm
M–N	–	–	427sm	434w	429w	432sm	435w	421w	433sm	415w	431sm

S strong, *sm* small, *w* weak, *m* medium, *br* broad

and resistant values. Blank paper discs (Schleicher and Schuell, Spain) with a diameter of 8.0 mm were impregnated with 10 μL of tested concentration of the stock solutions. When a filter paper disc impregnated with a tested chemical is placed on agar, the chemical will diffuse from the disc into the agar. This diffusion will place the chemical in the agar only around the disc. The solubility of the chemical and its molecular size will determine the size of the area of chemical infiltration around the disc. If an organism is placed on the agar, it will not grow in the area around the disc if it is susceptible to the chemical. This area of no growth around the disc is known as zone of inhibition or clear zone. For the disc diffusion, the zone diameters were measured with slipping calipers of the national committee for clinical laboratory standards [23]. Agar-based methods such E test and disc diffusion can be good alternatives because they are simpler and faster than broth based methods [24].

The following media were used in studying the antimicrobial properties of HSFX and HGly drugs and their complexes. The masses are given in gram per 1-L medium. Nutrient agar medium (pH 7.4) consists of beef extract (1.0 g), yeast extract (2.0 g), peptone (5.0 g), sodium chloride (5.0 g), agar (15.0 g) and distilled water (100 mL). Sabouraud's dextrose agar medium (pH 5.6) consists of peptone (10.0 g), dextrose (20.0 g), agar (15.0 g) and distilled water (100 mL). The data were repeated twice in order to check the accuracy of the test.

Results and discussion

The results of elemental analyses with molecular formulae of the chelates are listed in Table 1. The results obtained are in good agreement with that calculated for the suggested formulae. The results of elemental analyses suggest the formulae $[M(SFX)(Gly)(H_2O)_2]Cl$ (where M = Cr(III) and Fe(III), $[M(SFX)(Gly)(H_2O)_2]$ (where M = Mn(II), Co(II), Ni(II), Cu(II), Zn(II) and UO_2(II) and $[Th(SFX)(Gly)(H_2O)_2)]Cl_2$. The structures of the HSFX and HGly ligands under study are given in Fig. 1. The mass spectrum of HSFX ligand and possible molecular ion peaks with their respective relative intensity are shown in Scheme 1.

Characterization of metal complexes

Molar conductivity measurements

Table 1 shows the molar conductance values of the ternary complexes. From the molar conductivity of the ternary complexes, it is found that Fe(III) and Cr(III) ternary

Table 3 ^{1}H NMR spectral data of the HSFX and its Zn(II) ternary complex

Compound	Chemical shift, (δ)/ppm	Assignment
HSFX	13.5	(s, H, COOH)
	8.93	(m, H, CH of carbon 2)
	7.89	(d, 2H, NH_2)
	3.57	(d, 4H, CH_2 of carbon 5′, 6′)
	3.55	(d, 2H, CH_2 of carbon 2′)
	3.39	(d, H, CH of carbon 3′)
	3.12	(t, 2H, CH_2 of carbon 1b)
	3.10	(d, 3H, CH_3 of carbon 3a′)
	2.87	(d, H, CH of carbon 1a)
[Zn(SFX)(Gly)(H_2O)$_2$]	8.55	(s, H, CH of carbon 2)
	7.26	(d, 2H, NH_2)
	3.46	(d, 3H, CH, CH_2 of carbon 5′, 6′)
	3.42	(d, 2H, CH_2 of carbon 2′)
	3.26	(d, H, CH of carbon 3′)
	2.89	(t, 2H, CH_2 of carbon 1b)
	2.37	(d, 3H, CH_3 of carbon 3a′)

chelates have molar conductance value of 110 and 118 Ω^{-1} mol^{-1} cm^{-2}, respectively, indicating the ionic nature of these complexes. It also indicates the non bonding of the chloride anions to the Fe(III) and Cr(III) ions. So, the Fe(III) and Cr(III) chelates are considered as 1:1 electrolytes [25, 26]. On the other hand, ternary complexes of bivalent metal ions (Table 1) are found to have molar conductance values of 18.5, 22.2, 19.3, 21, 22.7 and 21.7 Ω^{-1} mol^{-1} cm^{-2} for Mn(II), Co(II), Ni(II), Cu(II), Zn(II) and UO_2(II) complexes, respectively. It is obvious from these data that these chelates are nonionic in nature and they are nonelectrolytes [25, 26]. The Th(IV) complex has a molar conductance value of 180 Ω^{-1} mol^{-1} cm^{-2} which indicates its ionic nature and it's 1:2 electrolyte [25, 26].

IR spectra and mode of bonding

The IR data of the HSFX, HGly and ternary chelate are listed in Table 2. The IR spectrum of HSFX ligand shows the υ(C=O) stretching vibration at 1,716 cm^{-1} as sharp intense band. This band is shifted to lower wave number (1,710–1,713 cm^{-1}) or disappeared in the complexes (Table 2) indicating the participation of carbonyl oxygen atom in coordination (M–O) [17]. The υ_{asym}(COO) and υ_{sym}(COO) stretching vibrations are observed at 1,532 and 1,332 cm^{-1}, respectively, for HSFX free ligand. The participation of the carboxylate O atom in the complexes formation is evidenced from shift in position of υ_{asym}(COO) and υ_{sym}(COO) stretching vibration bands from 1,532 cm^{-1} (free HSFX ligand) to 1,510–1,540 and from 1,332 cm^{-1} (free HSFX ligand) to 1,290–1,340 cm^{-1}, respectively, for ternary complexes [17].

The bands at 1,556 and 1,413 cm^{-1} region (Table 2), in the free Gly amino acid ligand are assigned to the antisymmetric and symmetric stretching vibrations of the carboxylate group, respectively [27]. The shift of these bands to higher or lower frequencies suggests the participation of –COOH group in complex formation after deprotonation [28]. The values of band shift $\Delta\upsilon(\upsilon_{asym}(COO)–\upsilon_{sym}(COO)$ are all about 160–193 cm^{-1}, indicating that the carboxylate group in HGly chelated in a monodentate manner to the metal ions with proton displacement [28]. At the wavenumber 3,000–3,500 cm^{-1} region of the ternary chelates, an overlap of the various υ(NH) vibrations coupled in many cases with molecules of water of hydration gives rise to very strong absorption. This prevents the individual recognition of the various bands. The asymmetric NH_2 stretching, NH_2 scissoring and NH_2 bending are found in the spectra of the free glycine ligand at 3400, 1613 and 698 cm^{-1}, respectively [27]. The participation of the NH_2 group in chelation is evidenced from the shift of the band to lower or higher wavenumbers to the extent of 12–30 cm^{-1}

Scheme 2 Zwitter-ion formation of HSFX

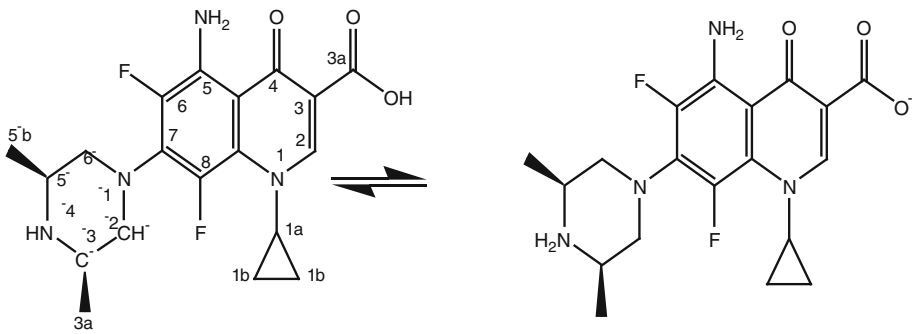

in all the complexes confirming coordination of the NH_2 group to the metal ions [29, 30] (Table 2).

New bands are found in the spectra of the complexes in the regions 504–527 and 442–460 cm^{-1} which are assigned to υ(M–O) stretching vibrations of carbonyl oxygen, carboxylate oxygen and coordinated water attachment to metal ions, respectively. The metal–oxygen stretching frequencies could not be assigned unambiguously due to the presence of three types of υ(M–O) vibrations, i.e. M–COO, M–H_2O and M–C=O. The bands at 415–435 cm^{-1} have been assigned to (M–N) stretching vibration. This is ensured the participation of amino group in the complex formation. Most of the band shifts observed at the wavenumber region care in agreement with the structural changes observed in the molecular carbon skelton after complexation, which cause some important changes in (C–C) bond lengths and also affect some of the C–O and C–N bonds indirectly [18, 31–33].

Most of the band shifts observed at the wavenumber region care in agreement with the structural changes observed in the molecular carbon skelton after complexation, which cause some important changes in (C–C) bond

Table 4 Thermoanalytical resutls (TG, DTG and DTA) of HSFX and the ternary complexes

Compound	TG range/°C	DTG_{max}/°C	n[a]	Mass loss/% calcd. (found)	Total mass/%	Fragment loss	Metallic residue	DTA[b]/°C
HSFX	150–380	266	1	75.79 (75.94)	99.66 (99.38)	Loss of $C_{17}H_{18}N_2O_3$	–	266(+), 401(+), 540(+)
	380–500	401	1	5.03 (5.09)		Loss of HF		
	500–850	540	1	18.84 (18.35)		Loss of C_2HFN_2		
(**1**)	30–150	51, 107, 137	1	5.82 (6.07)	86.11 (84.41)	Loss of HCl	1\2Fe_2O_3	51(−), 107(−), 137(−), 180(+), 346(+), 418(+), 474(+), 548(−)
	150–250	180	1	6.08 (5.72)		Loss of $2H_2O$		
	250–370	346	1	7.66 (7.43)		Loss of C_2H_6N		
	370–450	418	1	19.29 (19.41)		Loss of $C_5H_8FN_2$		
	450–850	474, 548	2	47.26 (47.78)		Loss of $C_{14}H_{10}FN_2O_{3.5}$		
(**2**)	30–150	41	1	6.38 (5.99)	85.58 (84.93)	Loss of $2H_2O$	NiO	41(+), 160(+), 337(−), 380(−), 480(+), 522(−)
	150–280	160	1	3.47 (3.57)		Loss of HF		
	280–350	337	1	27.14 (27.31)		Loss of $C_9H_{12}FN$		
	350–430	380	1	9.58 (9.99)		Loss of C_2H_2NO		
	430–700	480, 522	2	39.01 (39.07)		Loss of $C_{10}H_{10}N_3O_7$		
(**3**)	30–180	110	1	11.57 (10.96)	85.93 (87.15)	Loss of C_2H_4 and $2H_2O$	MnO	110(+), 320(+), 366(+), 480(−), 562(+), 603(+)
	180–380	320, 36	1	29.15 (29.47)		Loss of $C_7H_{15}FNO_2$		
	380–700	480, 562, 603	2	45.21 (46.72)		Loss of $C_{11}H_{11}FN_4O_2$		
(**4**)	30–280	150	1	12.36 (11.19)	87.46 (87.01)	Loss of HCl and $2H_2O$	1\2Cr_2 O_3	150(−), 315(−), 400(−), 464(+), 480(−), 566(+)
	280–390	315		27.98 (27.65)		Loss of $C_7H_{15}FN_2O$.		
	390–450	400	1	21.89 (21.71)		Loss of C_6H_7FNO		
	450–680	464, 480, 566	1	25.23 (26.46)		Loss of $C_8N_2O_{1.5}$		

(**1**) [Fe(SFX)(Gly)$(H_2O)_2$]Cl

(**2**) [Ni(SFX)(Gly)$(H_2O)_2$]

(**3**) [Mn(SFX)(Gly)$(H_2O)_2$]

(**4**) [Cr(SFX)(Gly)$(H_2O)_2$]Cl

[a] Number of decomposition steps

[b] (+) endothermic, (−) exothermic

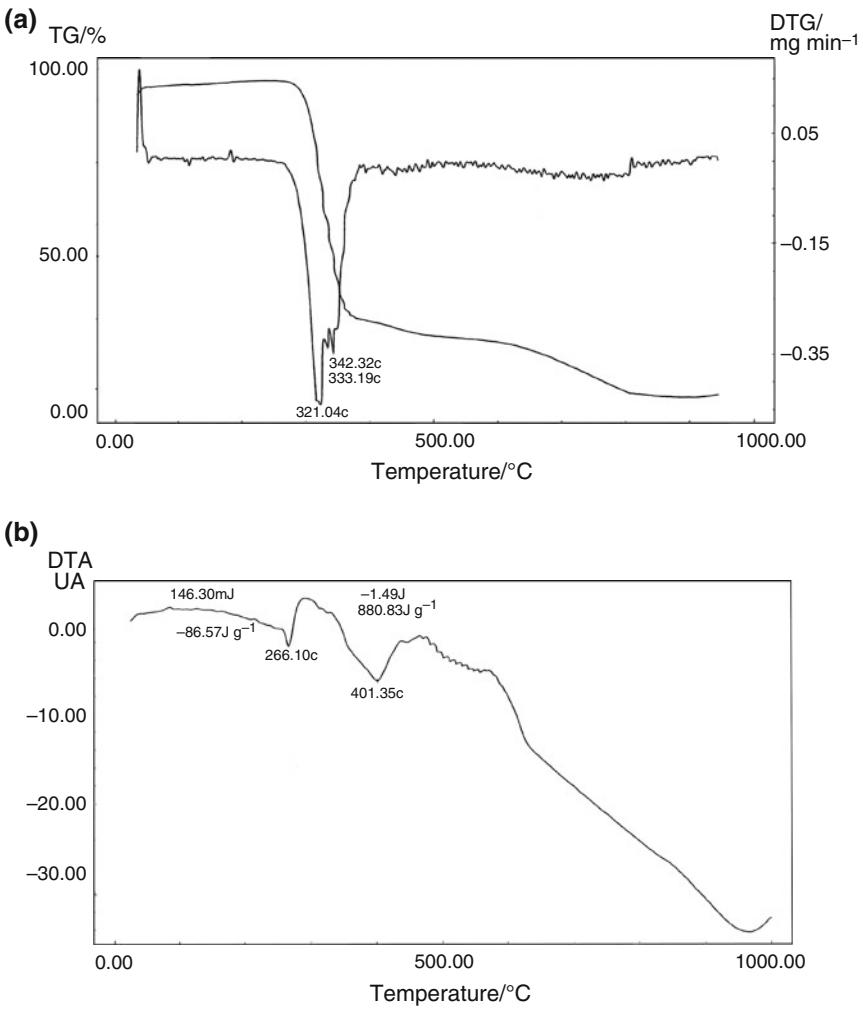

Fig. 2 **a** TG/DTG curve of SFX drug **b** DTA curve of SFX drug

lengths and also affect some of the C–O and C–N bonds indirectly [18, 31–33].

It is concluded that HSFX behaves as a uninegative bidentate ligand with OO donor coordination sites and coordinated to the metal ions via the carbonyl oxygen and deprotonated carboxlic oxygen. Glycine behaves as a uninegative bidentate ligand with NO donor sites and coordinated to the metal ion via the N amino group and deprotonated carboxylic oxygen.

^{1}H NMR spectral studies

The NMR spectra of HSFX, HGly and its Zn(II) complex were recorded in deuterated dimethylsulphoxide (DMSO-d_6) solution using tetramethylsilane (TMS) as internal standard. The chemical shifts of the different types of protons of the HSFX, HGly and diamagnetic Zn(II) complex are listed in Table 3. The spectrum of Zn(II) complex was compared with that of the parent HSFX ligand. Upon comparison with the free HSFX ligand, the signal observed at 13.5 ppm can be assigned to the carboxylate OH. This signal disappears in the spectra of the Zn(II) complex in accordance with the IR spectral data. Therefore, HSFX ligand coordinated to the metal ions with proton displacement and the disappearance of this signal can be attributed to Zwitter-ion formation shown in Scheme 2 [18, 31] in free state then followed by proton displacement upon complex formation with metal ions.

Magnetic susceptibility and diffused reflectance spectral studies

The $[Cr(SFX)(Gly)(H_2O)_2]Cl$ complex is found to have magnetic moment value of 3.95 B.M. The solid reflectance spectrum of the complex exhibits bands at 12384, 25094 and 27100 cm^{-1}, which assigned to $^{4}A_{2g} \rightarrow {}^{4}T_{2g}$, $^{4}A_{2g} \rightarrow {}^{4}T_{2g}$ and $^{4}A_{2g} \rightarrow {}^{4}T_{2g}(P)$ spin allowed d–d transitions, respectively. These bands suggest an octahedral geometry for the Cr(III) complex [34]. The diffused reflectance spectrum of the Mn(II) complex shows three bands at 14650, 19092 and

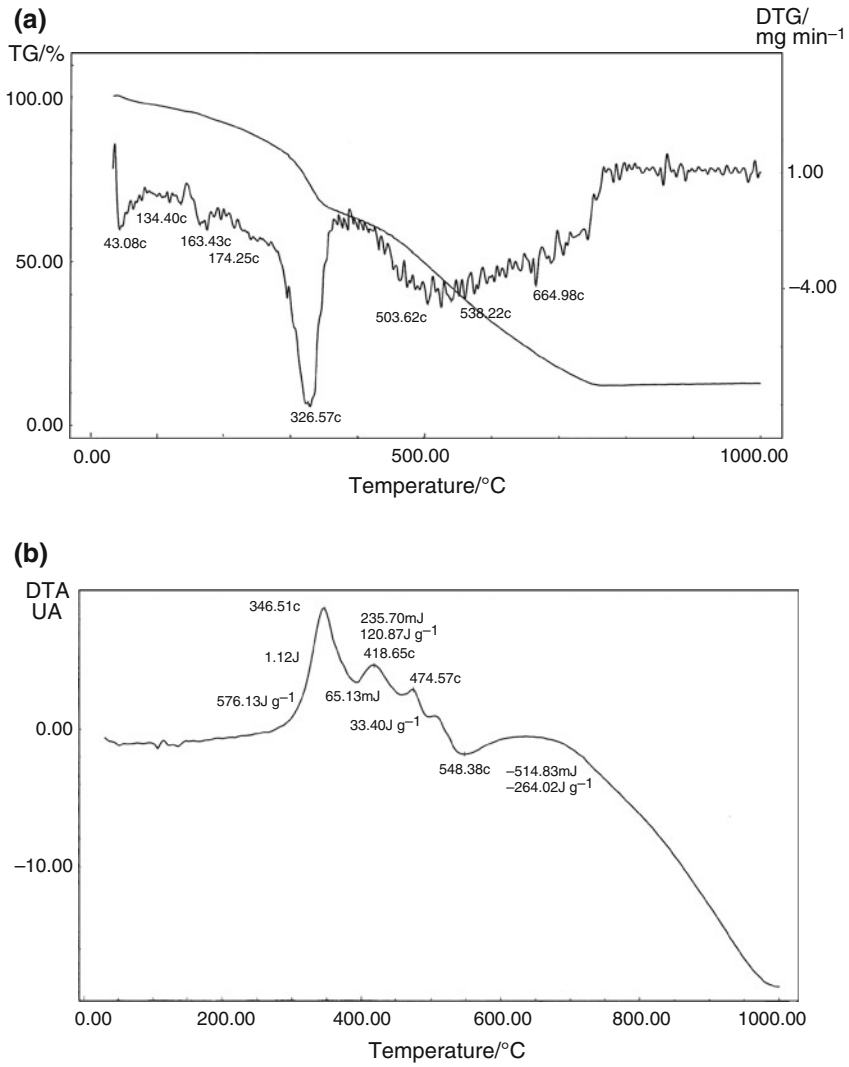

Fig. 3 **a** TG/DTG curve of [Fe (SFX)(Gly)$(H_2O)_2$Cl] complex, **b** DTA curve of [Fe (SFX)(Gly)$(H_2O)_2$Cl] complex

26631 cm^{-1} assignable to $^6A_{1g} \rightarrow {}^4T_{1g}$, $^6A_{1g} \rightarrow {}^4T_{2g}$(G) and $^6A_{1g} \rightarrow {}^4T_{1g}$(D) transitions, respectively [34]. The complex has magnetic moment value of 5.55 B.M. which confirm that the Mn(II) complex has an octahedral geometry. From the diffused reflectance spectrum it is observed that, the Fe(III) chelate exhibits band at 22,051 cm^{-1}, which may be assigned to the $^6A_{1g} \rightarrow T_{2g}$(G) transition in octahedral geometry of the complex [35]. The $^6A_{1g} \rightarrow {}^4T_{1g}$ transition appears to be split into two bands at 15,256 and 13,812 cm^{-1}. The observed magnetic moment value of Fe(III) complex is found to be 5.36 B.M. indicating octahedral geometry involving d^2sp^3 hybridization in Fe(III) ion [36]. The Co(II) complex has magnetic moment value of 5.74 B.M. indicating octahedral geometry [36]. The diffused reflectance spectra of the Co(II) complex gives three bands at 15481, 18069 and 22472 cm^{-1}. The bands observed are assigned to the $^4T_{1g}(F) \rightarrow {}^4T_{2g}(F)$ (ν_1), $^4T_{1g}(F) \rightarrow {}^4A_{2g}(F)$ (ν_2) and $^4T_{1g}(F) \rightarrow {}^4T_{1g}(P)$ (ν_3) transitions, respectively, suggesting that there is an octahedral geometry around Co(II) ion [37].

The studied Ni(II) complex is high spin with a room temperature magnetic moment value of 3.59 B.M. which is in the normal range observed for octahedral Ni(II) complexes [37]. Its diffused reflectance spectrum display three bands at 13596, 14035 and 20114 cm^{-1} which are assigned to $^3A_{2g}(F) \rightarrow {}^3T_{2g}(F)$ (ν_1), $^3A_{2g}(F) \rightarrow {}^3T_{1g}(F)$ (ν_2) and $^3A_{2g}(F) \rightarrow {}^3T_{1g}(P)$ (ν_3) transition, respectively [37]. The spectrum shows also a band at 25,608 cm^{-1} which may be attributed to ligand to metal charge transfer. The reflectance spectrum of the Cu(II) complex shows bands at 15,699 and 21,529 cm^{-1}. The ^3E_g and $^2T_{2g}$ states of the octahedral Cu(II) ion (d^9) split under the influence of the tetragonal distortion and the distortion can be such as to cause the three transitions $^2B_{1g} \rightarrow {}^2B_{2g}$, $^2B_{1g} \rightarrow {}^2E_g$ and $^2B_{1g} \rightarrow {}^2A_{1g}$ to remain unresolved in the spectrum [36, 37]. This assignment is in agreement with the general

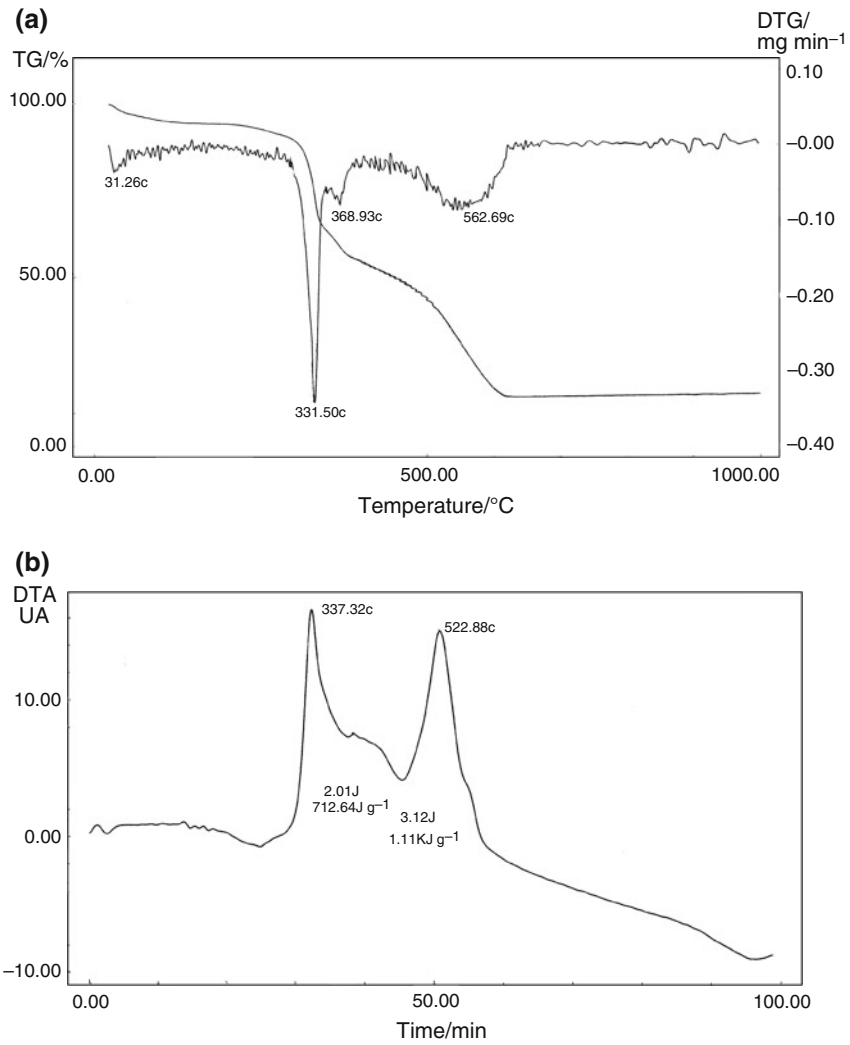

Fig. 4 **a** TG/DTG curve of $[Ni(SFX)(Gly)(H_2O)_2]$ complex, **b** DTA curve of $[Ni(SFX)(Gly)(H_2O)_2]$ complex

observation that Cu(II) d–d transitions are normally close in energy [36, 37]. The magnetic moment of this complex is 1.88 B.M., which fall within the range normally observed for octahedral Cu(II) complexes [38]. A moderately intense peak observed at 24,576 cm^{-1} is due to ligand to metal charge transfer transition. The Zn(II), The(IV) and UO_2(II) complexes are diamagnetic. According to their empirical formulae an octahedral geometry was proposed.

Thermal analyses (TG and DTG)

Several reports in the literature demonstrate the importance of thermal analysis by thermogravimetry (TG) and differential thermal analysis (DTA) in the characterization, polymorphism identification, purity evaluation of drugs, compatibility studies for the pharmaceutical formulation, stability and drugs thermal decomposition [39].

Table 4 shows the TG, DTG and DTA results of thermal decomposition of HSFX and the ternary metal chelates. The TG curve (Fig. 2a) of HSFX shows three successive steps of decomposition. The first estimated mass loss of 75.94 % (calcd. 75.79 %) at 150–380 °C may be attributed to the decomposition of $C_{17}H_{18}N_2O_3$ fragment loss. The second step within the temperature range from 380 to 500 °C, the estimated mass loss of 5.09 % (calcd. 5.03 %), may be attributed to loss of HF as gas fragment loss. In the final stage within the temperature range of 500–850 °C, the estimated mass loss of 18.35 % (calcd. 18.54 %), may be attributed to the decomposition of C_2HFN_2 fragment loss with a complete decomposition. DTA data are listed in Table 4 and represented graphically in Fig. 2b. It is clear from these data that these mass losses are accompanied by endothermic (266, 401 and 540 °C) peaks within the temperature range of decomposition from 150 to 850 °C. The peak at 266 °C represents the melting point of HSFX which is spontaneously accompanied by mass loss.

The curve of $[Fe(SFX)(Gly)(H_2O)_2]Cl$ chelate shows six decomposition steps within the temperature range of 30–850 °C as illustrated in Fig. 3a, b and Table 4. The first step of decomposition within the temperature range

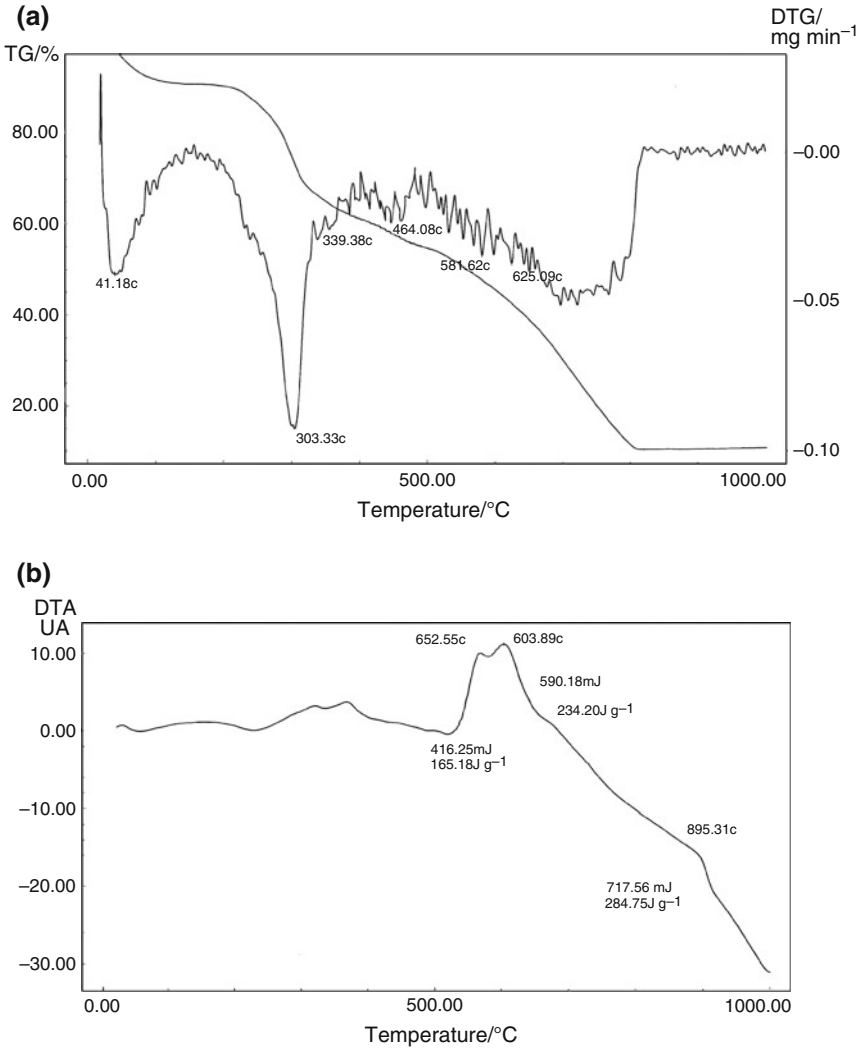

Fig. 5 **a** TG/DTG curve of [Mn (SFX)(Gly)$(H_2O)_2$] complex, **b** DTA curve of [Mn (SFX)(Gly)$(H_2O)_2$] complex

of 30–150 °C, corresponds to the loss of HCl fragment loss with amass loss of 6.07 % (calcd. 5.82 %). The second step corresponds to the loss of $2H_2O$ fragment loss with a mass loss of 5.72 % (calcd. 6.08 %) within temperature range 150–250 °C, but the third step of decomposition within the temperature range of 250–370 °C, shows loss of C_2H_6N fragment loss with a mass loss of 7.43 % (calcd. 7.66 %). The fourth step within the temperature range 370–450 °C shows loss of $C_5H_8FN_2$ fragment loss with amass loss 19.41 % (calcd. 19.29 %). The final stages within the temperature range from 450 to 850 °C, show loss of $C_{14}H_{10}FN_2O_{3.5}$ fragment loss with a mass loss of 47.78 % (calcd 47.26 %) leaving metal oxide as a residue (½Fe_2O_3). The DTA data are listed in Table 4 and represented in Fig. 3b. It is clear from these data that these mass losses are accompanied by exothermic peaks at 51, 107, 137 and 548 °C and endothermic peaks at 180, 346, 418 and 474 °C.

On the other hand, [Ni(SFX)(Gly)$(H_2O)_2$] complex exhibits six decomposition steps (Fig. 4a, b). The first step corresponds to the loss of $2H_2O$ fragment loss in the temperature range 30–150 °C with a mass loss 5.99 % (calcd. 6.38 %). The second step occurs within 150–280 °C and corresponds to the loss of HF mass loss 3.57 % (calcd. 3.47 %). The third step within temperature range of 280–350 °C shows loss of $C_9H_{12}FN$ (mass loss = 27.31 %; calcd. 27.14 %)]. The fourth step within the temperature range of 350–430 °C shows loss of C_2H_2NO fragment loss with a mass loss of 9.99 % (calcd. 9.58 %). The final stages within temperature range of 430–700 °C corresponds to the loss of $C_{10}H_{10}N_3O_5$ fragment loss (mass loss = 39.07 %, calcd. 39.01 %) and leaving metal oxide as a residue. The DTA data are listed

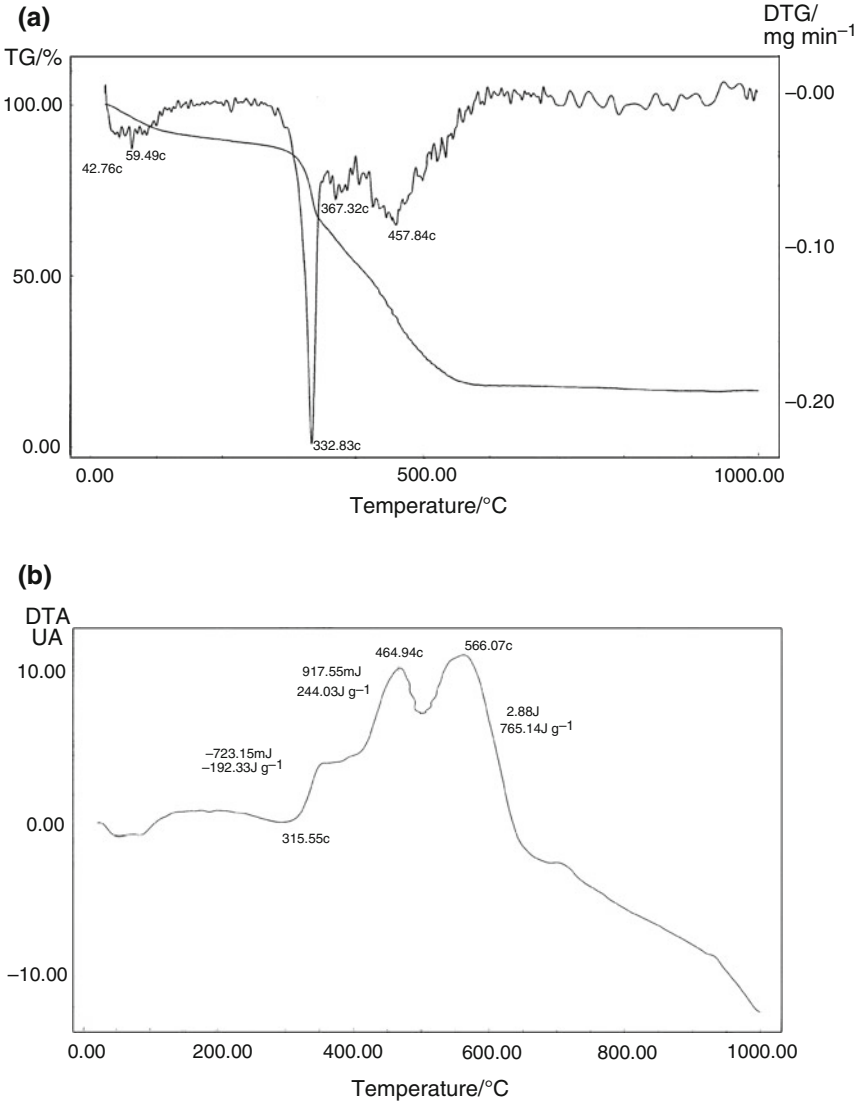

Fig. 6 **a** TG/DTG curve of $[Cr(SFX)(Gly)(H_2O)_2]$ complex, **b** DTA curve of $[Cr(SFX)(Gly)(H_2O)_2]$ complex

in Table 4 and represented graphically in Fig. 4b. It is clear from these data that these mass losses are accompanied by exothermic peaks at 337, 380 and 522 °C and endothermic peaks at 41, 160 and 480 °C.

The TG curve of $[Mn(SFX)(Gly)(H_2O)_2]$ chelate shows four decomposition steps within the temperature range 30–700 °C as illustrated in Fig. 5a, b and Table 4. The first step corresponds to the loss of C_2H_4 and $2H_2O$ fragment losses within temperature range 30–180 °C with mass loss of 10.96 % (calcd. 11.57 %). The second step takes place within the temperature range of 180–380 °C and shows loss of $C_7H_{15}FNO_2$ with mass loss 29.47 % (calcd. 29.15 %). The final stages within the temperature range of 380–700 °C corresponds to the removal of the organic part of the ligands ($C_{11}H_{11}FN_4O_2$) leaving metal oxide as a residue with mass loss of 46.72 % (calcd. 45.21 %). The DTA data are listed in Table 4 and represented graphically in Fig. 5b. It is clear from these data that these mass losses are accompanied by endothermic peaks at 110, 320, 366, 562 and 603 °C and exothermic peak at 480 °C.

On the other hand $[Cr(SFX)(Gly)(H_2O)_2]Cl$ exhibit six decomposition steps (Fig. 6a, b). The first step corresponds to the loss of HCl and $2H_2O$ fragment loss in the temperature range of 30–280 °C with mass loss 11.19 % (calcd. 12.36 %). The second stage (280–390 °C) corresponds to the loss of part of organic ligand ($C_7H_{15}FN_2O$ fragment loss) with mass loss 27.65 % (calcd 27.98 %). The third stage at 390–450 °C can be attributed to the loss of C_6H_7FNO fragment loss with mass loss of 21.71 % (calcd. 21.89 %). The final stages correspond to the removal of the organic part of the ligand ($C_6N_2O_{3.5}$ molecule) leaving metal oxide as a residue with mass loss of 26.46 % (calcd. 25.23 %) in the temperature range 450–680 °C. The DTA data are listed Table 4 and represented graphically in

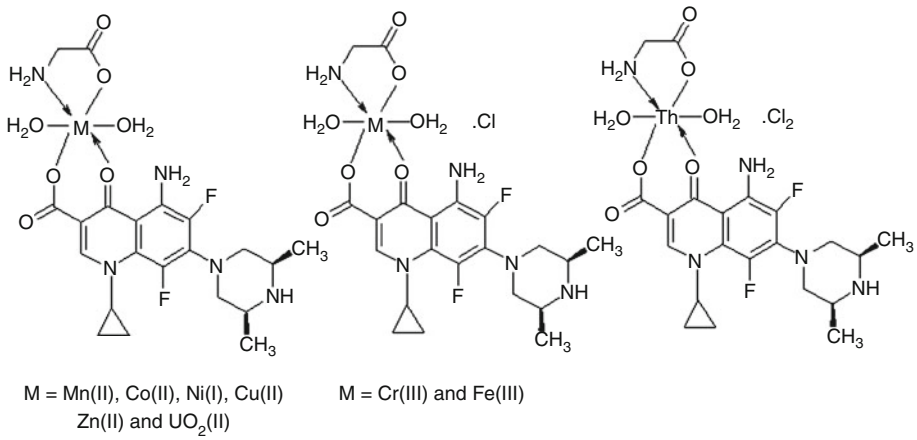

Fig. 7 Structure of ternary complexes

Fig. 6b. It is clear from these data that these mass losses are accompanied by exothermic peaks at 150, 315, 400 and 480 °C and endothermic peaks at 464 and 566 °C.

Structural interpretation

Based on the various physicochemical and spectral data presented and discussed in this article, the ternary complexes may be suggested to have octahedral geometry and their structures are shown in Fig. 7.

Biological activity

Therefore, there is need for having a chemotherapeutic agent which controls only one function. In testing the antibacterial and antifungal activity of these compounds, more than one test organism was used to increase the chance of detecting antibiotic principles in tested materials. All of the tested compounds show a remarkable biological activity against different types of Gram-positive (G^+) and Gram-negative (G^-) bacteria and also fungi. The data are listed in Table 5.

The comparison of the biological activity of the HSFX, HGly and ternary metal complexes with the tetracycline (antibacterial agent) and amphotericin B (antifungal agent) standards, towards the different organisms brings out the following facts to light. The free HSFX ligand and its respective ternary metal chelates with HGly were screened against *Candida albicans*, *Aspergillus flavus*, *Staphylococcus aureus* (G^+) and *Escherichia coli* (G^-) bacteria to asses their potential antimicrobial activity.

Table 5 Biological activity of ternary HSFX, HGly and the ternary complexes

Sample	Inhibition zone diameter mm mg^{-1} sample			
	Escherichia coli	*Staphylococcus aureus*	*Aspergillus flavus*	*Candida albicans*
Control				
DMSO	0.0	0.0	0.0	0.0
HSFX	42	47	0.0	0.0
HGly	10	9	0.0	10
$[Cr(SFX)(Gly)(H_2O)_2]\cdot Cl$	35	43	0.0	12
$[Mn(SFX)(Gly)(H_2O)_2]$	41	48	0.0	0.0
$[Fe(SFX)(Gly)(H_2O)_2]Cl$	35	35	0.0	11
$[Co(SFX)(Gly)(H_2O)_2]$	36	42	0.0	0.0
$[Ni(SFX)(Gly)(H_2O)_2]$	35	40	0.0	22
$[Cu(SFX)(Gly)(H_2O)_2]$	40	35	0.0	12
$[Zn(SFX)(Gly)(H_2O)_2]$	40	37	0.0	0.0
$[Th(SFX)(Gly)(H_2O)_2]\cdot Cl_2$	38	40	0.0	12
$[UO_2(SFX)(Gly)(H_2O)_2]$	30	31	0.0	13
Standard				
Tetracycline (antibacterial agent)	33	31	–	–
Amphotericin B (antifungal agent)	–	–	16	19

It is clear from Table 5 that HSFX, HGly and all the ternary complexes have no fungal activity towards *Aspergillus flavus* organism. The biological activity against *Candida albicans* shows that Co(II), Zn(II) and Mn(II) ternary complexes together with HSFX ligand have no fungal activity. The remaining ternary complexes are found to have fungal activity and the order of activity is: Ni(II) > UO_2(II) > Th(IV) = Cr(III) = Cu(II) > Fe(III). It is obvious also that Ni(II) ternary complex have higher fungal activity than the standard. Also, the data in Table 5 show that the biological activity of HSFX and the ternary metal complexes towards *Staphylococcus aureus* (G^+) bacteria have the order Mn(II) > HSFX > Cr(III) > Co(II) > Th(IV) = Ni(II) > Zn(II) > Fe(III) = Cu(II) > UO_2(II) = tetracycline standard > HGly. For *Escherichia coli* (G^-) bacteria, the ternary complexes were found to have the activity in the order HSFX > Mn(II) > Cu(II) = Zn(II) > Th(IV) > Co(II) > Cr(III) = Fe(III) = Ni(II) > tetracycline standard > UO_2(II) > HGly. It is obvious from these results that HSFX drug and all the metal complexes have bacterial activity more than the standard except UO_2(II) ternary complex. Also the complexes have nearly comparable biological activity like that of the parent HSFX drug.

Conclusions

The synthesis and the characterization of nine novel mononuclear M(II)/(III)/(IV) complexes with the third-generation quinolone antibacterial drug HSFX in the presence of a nitrogen-donor ligand HGly, has been realized with physicochemical, spectroscopic and thermal methods. In all these complexes, the HSFX ligand is bound to metal ions via the pyridone oxygen and one carboxylate oxygen. While, HGly behaves as uninegative bidentate ligand coordinated to the metal ions via deprotonated carboxylate O and amino N atoms. The results of this investigation support the suggested octahedral structure of the metal complexes and form a favourable molecular arrangement. The thermal behaviour of the complexes revealed that they decomposed in three to six steps within the temperature range 30–1,000 °C they loss water molecules in the first steps followed by the decomposition of the HSFX and HGly molecules in the subsequent steps. Based on these facts, the ternary metal complexes were found to be highly active against the antibacterial and antifungal species. The antimicrobial activity results show that most of the synthesized complexes possess good antibacterial activity against Gram-negative and Gram-positive bacteria tested and the microbial activity of the complexes in most cases is higher than that of the corresponding HSFX and glycine ligands.

Acknowledgements The authors wish to express their deep thanks for Mr/Ahmed Abou El-Alameen for carrying out the biological activity study in this work.

References

1. Lohray BB, Lohray VB, Srivastava BK, Kapadins PB, Pandya PP. Novel tetrahydro-thieno pyridyl oxazolidinone: an antibacterial agent. J Bioorg Med Chem. 2004;12:4557–64.
2. Aronson JK. Sparfloxacin in Meyler's side effects of drugs: International Encycopedia of adverse dry reactions and interactions. Elsevier: Oxford; 2006. p. 3172–4.
3. Xiao S-X, Li A-T, Li C-H, Xiao H-Y, Xu X-Y, Li Q-G. Determination of the standard molar enthalpy of formation of the ternary complex of neodymium with vitamin B3 and 8-hydroxyquinoline by microcalorimetry. J Therm Anal Calorim. 2013;112:1533–8.
4. Gaber M, El-Hefnawy GB, El-Borai MA, Mohamed NF. Synthesis, spectral and thermal studies of Mn(II), Co(II), Ni(II), Cu(II) and Zn(II) complex dyes based on hydroxyquinoline moiety. J Therm Anal Calorim. 2012;109:1397–405.
5. Turel I. The interaction of metal ions with quinolone antibacterial agents. J Coord Chem Rev. 2002;272:27–47.
6. Xiao S-X, Jiang J-H, Li X, Li Y, Li Q-G. Thermochemical properties of the coordination complex of 8-hydroxyquinolinato-bis-(salicylato) praseodymium(III). J Therm Anal Calorim. 2013;113:1139–44.
7. Jain S, Jain NK, Pitre K. Electrochemical analysis of sparfloxacin in pharmaceutical formulation and biochemical screening of its Co(II) complex. J Pharm Biomed Anal. 2002;29:795–801.
8. Vieira LM, De Almeida MV, De Abreu HA, Duarte HA, Grazul RM, Fontes AP. Platinum(II) complexes with fluoroquinolones: synthesis and characterization of unusual metal piperazine chelates. J Inorg Chim Acta. 2009;362:2060–4.
9. Anacona JR, Totedo C. Synthesis and antibacterial activity of metal complexes of ciprofloxacin. J Trans Met Chem. 2001;26:228–31.
10. Sultana N, Saeed M, Gul S, Shamim S. Sparfloxacin-metal complexes as antifungal agents: their synthesis, characterization and antimicrobial activities. J Mol Struct. 2010;975:285–91.
11. El-Gamel NE, Mohamed RR, Zayed MA. Synthesis, characterization of enrofloxacine complexes as thermal stabilizers for rigid poly (vinyl chloride). J Dalton Trans. 2012;41:1824–31.
12. Sarin R, Mushi KN. Thermodynamics of complex formation of indium metal ion with mercapto, hydroxy and amino substituted succinic acid. J Inorg Nucl Chem. 1972;34:581–90.
13. Refat MS, Mohamed GG. Ti(IV), Cr(III), Mn(II), and Ni(II) complexes of the norfloxacin antibiotic drug: spectroscopic and thermal characterizations. J Chem Eng Data. 2010;55(9):3239–46.
14. Mohamed GG, Abd El-halim HF, El-Dessouky MMI, Mahmoud WH. Synthesis and characterization of mixed ligand complexes of lomefloxacin drug and glycine with transition metals. Antibacterial, antifungal and cytotoxicity studies. J Mol Struct. 2011;999(1–3):29–38.
15. Abd El-halim HF, Mohamed GG, El-Dessouky MMI, Mahmoud WH. Ligational behaviour of lomefloxacin drug towards Cr(III), Mn(II), Fe(III), Co(II), Ni(II), Cu(II), Zn(II), Th(IV) and UO_2(VI) ions: synthesis, structural characterization and biological activity studies. Spectrochim Acta Part A. 2011;82(1):8–19.
16. Abd El-halim HF, Mohamed GG, El-Dessouky MMI, Mahmoud WH. Cr(III), Mn(II), Fe(III), Co(II), Ni(II), Cu(II), Zn(II), Th(IV) and UO_2(II) mixed ligand complexes of lomefloxacin and DL-alanine preparation, spectroscopic characterization, biological and anticancer activity. J Pharm Res. 2012;5(11):5084–92.

17. Refat MS, Mohammed GG, De Farias RF, Powell AK, El-Garib MS, El-Karashy SA, Hussien MA. Spectroscopic, thermal and kinetic studies of coordination compounds of Zn(II), Cd(II) and Hg(II) with norfloxacin. J Therm Anal Calorim. 2010;102: 225–32.
18. Refat MS. Synthesis and characterization of norfloxacin-transition metal complexes (group 11, IB): spectroscopic, thermal, kinetic measurements and biological activity. Spectrochim Acta Part A. 2007;68:1393–405.
19. Bauer AW, Kirby WM, Sherris C, Turc KM. Antibiotic susceptibility testing by a standardized signal disc method. Am J Clin Pathol. 1966;45:493–9.
20. Pfaller MA, Burmeister L, Bartlett MA, Rinaldi MG. Multicancer evaluation of four methods of yeast inoculum preparation. J Clin Microb. 1988;26:1437–41.
21. National Committee for Clinical Laboratory Standard. Reference method for borth dilution antifungal susceptibility testing of conidium-forming filamentous: proposed standard M38-A. Wayne, PA, USA. 2002.
22. National Committee for Clinical Laboratory Standards. Method for antifungal disc diffusion susceptibility testing of yeast: proposed guideline M 44-P, Wayne, PA, USA. 2003.
23. Liebowitz LD, Ashbee HR, Evans EG, Chong Y, Mallatova N, Zaidi M, Gibbs D. Global surveillance group. J Microbiol Infect Dis. 2001;4:27–33.
24. Matar MJ, Zeichner LO, Paetzink VL, Rodriguez JR, Chen E, Rex JH. Correlation between *E*-test, disc diffusion and microdilution methods for antifungal susceptibility testing of fluconazole and voriconazole. J Agents Chemother. 2003;47:1647–51.
25. Geary WJ. The use of conductivity measurements in organic solvents for the characterization of coordination compounds. Coord Chem Rev. 1971;7:81–122.
26. Sece HJ, Quiros M, Garmendia MJ. Synthesis, x-ray crystal structure and spectroscopic, magnetic and EPR studies of copper (II) dimmers with methoxy-di-(2-pyridyl) methoxide as bridging ligand. Polyhedron. 2000;19:1005–13.
27. Kumar S, Rai A, Rai SB, Rai DK, Singh AN, singh VB. Infrared, Raman and electronic spectra of alanine: a comparison with ab intio calculation. J Mol Struct. 2006;791:23–9.
28. Kumar S, Rai A, Rai SB, Ria DK, Singh VB. Vibrational spectrum of glycine molecule. J Spectrochim Acta Part A. 2005; 61:2741–6.
29. Olie GH, Olive S. The chemistry of the catalyses hydrogenation of carbon monoxide. Berlin: Springer; 1984.
30. Mohammed GG, Soliman AA. Study of the ternary complexes of copper with salicylidene-2-aminothiophenol and some amino acids in the solid state. Thermochim Acta. 2004;421:151–9.
31. Sandhu GK, Verma SP. Triorgano tin(IV) derivatives of five membered he terocyclic-2-carboxylic acids. Polyhedron. 1987;6: 587–92.
32. Aletras V, Hadjiliadis N, Lippert B. Ternary complexes of trans-$Pt(NH_3)_2Cl_2$ with amino acids and nucleo bases. Polyhedron. 1992;11:1359–67.
33. Zidan AS, El-Said AI, El-Meligy MS, Aly AA, Mohamed OF. Mixed ligand complexes of 5-arylazo-8-hydroxyl quinoline and α-amino acids with Co(II), Ni(II) and Cu(II). J Therm Anal Calorim. 2000;26:665–79.
34. Martin RB, Sigel H. Quantification of intramolecular ligand equilibria in metal–ion complexes. Comments Inorg Chem. 1988;6:285–314.
35. Mohammed GG, Soliman MH. Synthesis, spectroscopic and thermal characterization of sulpiride complexes of iron, manganese, copper, cobalt, nickel and zinc salts. Antibacterial and antifungal activity. Spectrochim Acta Part A. 2010;76:341–7.
36. Mohammed GG, Omar MM, Ibrahim AA. Preparation, characterization and biological activity of novel metal-NNNN donor Schiff base complexes. Spectrochim Acta Part A. 2009;73: 358–69.
37. Mondal N, Dey DK, Mitra S, Abdul Malik KM. Kinetic parameters from thermogravimetric data. Polyhedron. 2000;19:2707–11.
38. Mohammed GG, Omar MM, Ahmed MM. Synthesis, characterization and biological activity of some transition metals with Schiff base derived from 2-thiophene carboxaldehyde and aminobenzoic acid. Spectrochim Acta Part A. 2005;62:1140–50.
39. Yoshida MI, Gomes ECL, Soares CDV, Cunha AF, Oliveira MA. Thermal analysis applied to verapamil hydrochloride characterization in pharmaceutical formulations. Molecules. 2010;15: 2439–52.